J. Cent. South Univ. (2012) 19: 578−585
DOI: 10.1007/s11771−012−1042−1

Springer

Wing crack model subjected to high hydraulic pressure and far field stresses and its numerical simulation

ZHAO Yan-lin(赵延林)[1, 2, 3], CAO Ping(曹平)[3], WANG Wei-jun(王卫军)[1, 2], WAN Wen(万文)[1,2], CHEN Rui(陈锐)[3]

1. School of Energy and Safety Engineering, Hunan University of Science and Technology, Xiangtan 411201, China;
2. Hunan Provincial Key Laboratory of Safe Mining Techniques of Coal Mines, Hunan University of Science and Technology, Xiangtan 411201, China;
3. School of Resources and Safety Engineering, Central South University, Changsha 410083, China

Abstract: By considering the effect of hydraulic pressure filled in wing crack and the connected part of main crack on the stress intensity factor at wing crack tip, a new wing crack model exerted by hydraulic pressure and far field stresses was proposed. By introducing the equivalent crack length l_{eq} of wing crack, two terms make up the stress intensity factor K_I at wing crack tip: one is the component $K_I^{(1)}$ for a single isolated straight wing crack of length $2l$ subjected to hydraulic pressure in wing crack and far field stresses, and the other is the component $K_I^{(2)}$ due to the effective shear stress induced by the presence of the equivalent main crack. The FEM model of wing crack propagation subjected to hydraulic pressure and far field stresses was also established according to different side pressure coefficients and hydraulic pressures in crack. The result shows that a good agreement is found between theoretical model of wing crack proposed and finite element method (FEM). In theory, an unstable crack propagation is shown if there is high hydraulic pressure and lateral tension. The wing crack model proposed can provide references for studying on hydraulic fracturing in rock masses.

Key words: rock mechanics; wing crack; hydraulic pressure; numerical simulation

1 Introduction

The slippage, propagation and interaction of joint fissures in rock masses, under engineering load, have significant influence on the mechanical properties of rock masses, leading to final failure [1−3]. In the rock masses, slip-split failure generally occurs under uniaxial compression or low confining pressure [4]. As frictional force is overcome by shear stress induced by far-field stresses on the crack surface, the crack surface would slide over each other, causing stress concentration on tip of crack and leading to the initiation and splitting propagation of wing crack finally [5]. Different calculation models of wing crack propagation and stress intensity factor at the tip of wing crack have been proposed by HORII and NEMAT-NASSER [5−6], ASHBY and HALLAM [7], STEIF [8], BAUD et al [9], and WANG et al [10], based on different types of hypothesises in last several decades. Many factors, like the direction of main crack surface, orientation of the wing crack propagation, lateral stress and friction coefficient of the main crack surface, were taken into consideration in the wing crack models proposed comprehensively. However, hydraulic pressure in cracks is ignored in the mentioned wing crack models above. Rock masses strength can be greatly influenced by hydraulic load because of the complex geological environment. In the macroscopic view, effective normal stress on the crack surface is reduced by hydraulic pressure, causing the aggravation of the tendency that rock masses slide along the crack surface. In the microscopic view, the stress intensity factor of crack is enhanced and the splitting propagation is exacerbated by hydraulic pressure that penetrates into wing crack after wing crack propagates. Some efforts were conducted by scholars to study the hydraulic pressure effect on fracture mechanical properties of rock masses. The effects of hydrostatic pressure, hydrodynamic pressure and hydrochemistry damage on stress intensity factor of crack tip were studied by NAKASHIMA [11] and TANG et al [12]. The law of propagation of rock masses cracks

Foundation item: Projects(10972238, 51074071, 50974059) supported by the National Natural Science Foundation of China; Project(10JJ3007) supported by the Natural Science Foundation of Hunan Province, China; Project(11C0539) supported by Scientific Research Fund of Hunan Provincial Education Department, China; Project(200905) supported by Open Research Fund of Hunan Provincial Key of Safe Mining Techniques of Coal Mines, China
Received date: 2010−09−26; **Accepted date:** 2011−04−13
Corresponding author: ZHAO Yan-lin, PhD; Tel: +86−13974963257; E-mail: yanlin_8@tom.com

in coupling process of hydraulic pressure and stress was studied by ZHUANG [13] by using PFC software. And a series of injection-induced slip experiments using pre-fractured granitic rock specimens to investigate the dynamic hydraulic responses of existing fractures during hydraulic stimulation were conducted by KATSUMI et al [14]. But, there is no reasonable model for evolution laws of stress intensity factor at wing crack tip subjected to hydraulic pressure and far field stresses [15−17]. New wing crack model subjected to hydraulic pressure and far field stresses was proposed by considering the effect of hydraulic pressure on the main crack and wing crack. And the numerical simulation of wing crack propagation was also made using ANSYS software. The theoretical model of wing crack was proposed to provide references for studying on hydraulic fracture in fractured rock masses, which allows extended numerical applications [18].

2 Wing crack model subjected to hydraulic pressure and far-field stresses

For the purpose of studying the laws of initiation and propagation of frictional crack, the following hypotheses have been proposed:

1) Connectivity rate of main crack is α, and the main crack is partially close. Accordingly, the effective hydraulic pressure of main crack changes to αp. And the distributed force $F=\alpha p$ is applied to main crack surface (as shown in Fig. 1);

2) When water enters into wing crack, wing crack propagating becomes a distributed force applied to wing crack surface (as shown in Fig. 1).

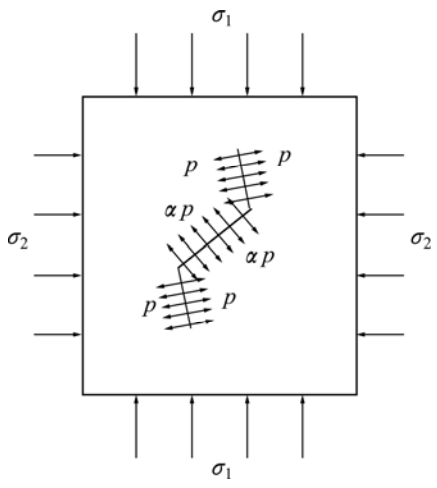

Fig. 1 Sketch illustrating hydraulic pressure applied to main crack and wing crack

2.1 Initiation of frictional main crack

The normal ($\sigma_{n,e}$) and shear ($\tau_{n,e}$) stresses are derived on the crack plane:

$$\begin{cases}\sigma_{n,e}=\sigma_n-\beta p=(\sigma_1\cos^2\beta+\sigma_2\sin^2\beta)-\alpha p\\ \tau_{n,e}=\dfrac{\sigma_1-\sigma_2}{2}\sin 2\beta\end{cases} \quad (1)$$

where β is the angle between crack surface and direction of the maximum main stress σ_1.

Effective shear stress (τ_{eff}) suggested by many studies [19−22] is the only stress component that leads to stress singularity at the tip of the frictional crack:

$$\tau_{eff}=\tau_{n,e}-\mu\sigma_{n,e} \quad (2)$$

where μ is the friction coefficient of crack surface.

Model II factor K_{II} is the stress intensity factor which appears at main crack tip:

$$K_{II}=\tau_{eff}\sqrt{\pi a} \quad (3)$$

Wing crack propagates as effective shear stress (τ_{eff}) reaches the critical value, but not on its own plane. A wing crack propagates from the tip of initial crack in a direction θ at which the transformed mode I stress intensity factor $K_I(\theta)$ is at a maximum and greater than the fracture toughness K_{IC} of rock material, the critical stress intensity factor in mode I. The transformed stress intensity factor is given by [9]

$$K_I(\theta)=\frac{3}{2}K_{II}\cos\theta\cos\frac{\theta}{2} \quad (4)$$

We can obtain θ=70.5° by supposing that wing crack propagates along the maximum value of $K_I(\theta)$, then

$$K_I=\frac{2}{\sqrt{3}}\tau_{eff}\sqrt{\pi a} \quad (5)$$

When $K_I\geq K_{IC}$, frictional main crack initiates.

2.2 Wing crack model

When $K_I\geq K_{IC}$, wing crack initiates then propagates at tip of the main crack. The stress intensity factor of wing crack varies with the propagation of wing crack. The propagation of wing crack terminates when stress intensity factor K_I at wing crack tip is lower than K_{IC}, namely $K_I<K_{IC}$. For the purpose of studying the evolution law of stress intensify factor at wing crack tip, many wing crack models are proposed, based on different hypotheses. However, the effect of hydraulic pressure is lack of consideration. In this work, the new wing crack model subjected to hydraulic pressure and far field stresses is proposed.

Stress intensify factor K_I at tip of wing crack is presumed to be the sum of two terms as shown in Fig. 2.

1) A component $K_I^{(1)}$ for the two straight wing cracks, of common length l, regarded as a single isolated straight crack of length $2l$, and subjected to hydraulic pressure in wing crack and far field stresses;

2) A component $K_I^{(2)}$ due to effective shear stress induced by the presence of the main crack subjected to hydraulic pressure in main crack and far field stresses.

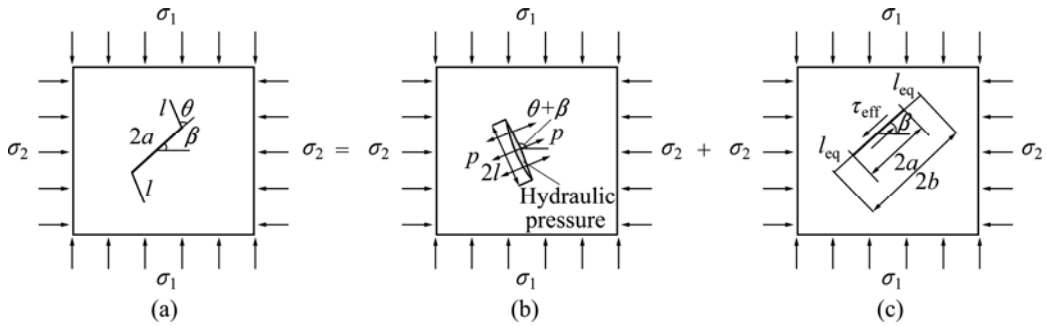

Fig. 2 Superposition technique used to calculate K_I at wing crack tip subjected to hydraulic pressure and far field stresses: (a) Approximate K_I at wing crack tip; (b) $K_I^{(1)}$ for straight wing crack of common length $2l$; (c) $K_I^{(2)}$ due to effective shear stress induced by presence of main crack

For the purpose of calculating $K_I^{(2)}$, we replace the system (main crack−wing crack pair) by an equivalent single straight crack of length $2b$ and the same orientation β as the initial main crack. Equivalent single straight crack of length $2b$ is assumed to be the sum of two terms: the first part, the main length $2a$, and the second part, the equivalent wing crack length of $2l_{eq}$, where l_{eq} is the function of wing crack length l, orientation θ and main crack length a.

$$2b = 2a + 2l_{eq} \tag{6}$$

Because the wing crack propagates in such a direction that small shear stress is applied to it, the equivalent wing crack length of $2l_{eq}$ should also be seen as free shear stress.

Stress intensify factor K_I at tip of wing crack can be expressed as

$$K_I = K_I^{(1)} + K_I^{(2)} \tag{7}$$

The term $K_I^{(1)}$ in Eq. (7), as shown in Fig. 2(b), is determined by the following equations:

$$\sigma_n' = \frac{1}{2}[(\sigma_1+\sigma_2)+(\sigma_1-\sigma_2)\cos 2(\theta+\beta)] \tag{8}$$

$$K_I^{(1)} = -(\sigma_n' - p)\sqrt{\pi l} = -\frac{1}{2}[(\sigma_1+\sigma_2)+ (\sigma_1-\sigma_2)\cos 2(\theta+\beta) - 2p]\sqrt{\pi l} \tag{9}$$

The stress intensify factor of the equivalent straight crack induced by the effective shear stress is given by [9]

$$K_{II} = 2\tau_{eff}\sqrt{\frac{a+l_{eq}}{\pi}}\sin^{-1}\left(\frac{a}{a+l_{eq}}\right) \tag{10}$$

The transformed stress intensify factor $K_I^{(2)}$ of equivalent straight crack with orientation of θ can be obtained from Eq. (4):

$$K_I^{(2)} = 3\tau_{eff}\sqrt{\frac{a+l_{eq}}{\pi}}\sin^{-1}\left(\frac{a}{a+l_{eq}}\right)\sin\theta\cos\frac{\theta}{2} \tag{11}$$

Using Eqs. (9) and (11), K_I can be expressed as

$$K_I = 3\tau_{eff}\sqrt{\frac{a+l_{eq}}{\pi}}\sin^{-1}\left(\frac{a}{a+l_{eq}}\right)\sin\theta\cos\frac{\theta}{2} - (\sigma_n' - p)\sqrt{\pi l} \tag{12}$$

For the purpose of determining equivalent wing length l_{eq}, wing crack model proposed by HORRI and NEMAT-NASSER [6] is introduced:

$$K_I = \frac{2a\tau_{eff}\sin\theta}{\sqrt{\pi(l+l^*)}} - \sigma_n'\sqrt{\pi l} \tag{13}$$

Then, a parameter l^*=0.27a is added to obtain proper behavior at little wing crack limit.

Taking hydraulic pressure applied to the main crack and wing crack into consideration, HORRI and NEMAT-NASSER model is modified as

$$K_I = \frac{2a\tau_{eff}\sin\theta}{\sqrt{\pi(l+l^*)}} - (\sigma_n' - p)\sqrt{\pi l} \tag{14}$$

Via comparing Eqs. (12) and (14), Eq. (15) can be obtained:

$$3\tau_{eff}\sqrt{\frac{a+l_{eq}}{\pi}}\sin^{-1}\left(\frac{a}{a+l_{eq}}\right)\sin\theta\cos\frac{\theta}{2} = \frac{2a\tau_{eff}\sin\theta}{\sqrt{\pi(l+0.27a)}} \tag{15}$$

Considering the condition that the crack length is rather short $l \to 0$, from Eq. (15), we obtain the following equation:

$$\lim_{l\to 0} 3\tau_{eff}\sqrt{\frac{a+l_{eq}}{\pi}}\sin^{-1}\left(\frac{a}{a+l_{eq}}\right)\sin\theta\cos\frac{\theta}{2} = \frac{3\pi}{2}\tau_{eff}\sqrt{\frac{a+l_{eq}}{\pi}}\sin\theta\cos\frac{\theta}{2} \tag{16}$$

By using Eqs. (15) and (16), l_{eq} can be expressed as

$$l_{eq} = \left(\frac{0.667}{\cos^2(0.5\theta)} - 1\right)a \tag{17}$$

Considering the condition that the crack length is extremely long $l\to\infty$, the following formula can be obtained by identifying Eq. (15):

$$\lim_{l\to\infty} 3\tau_{\text{eff}}\sqrt{\frac{a+l_{\text{eq}}}{\pi}}\sin^{-1}\left(\frac{a}{a+l_{\text{eq}}}\right)\sin\theta\cos\frac{\theta}{2}= 3\tau_{\text{eff}}\sqrt{\frac{a+l_{\text{eq}}}{\pi}}\frac{a}{a+l_{\text{eq}}}\sin\theta\cos\frac{\theta}{2} \tag{18}$$

By using Eqs. (15) and (18), l_{eq} can be expressed as

$$l_{\text{eq}}=\frac{9}{4}l\cos^2\frac{\theta}{2} \tag{19}$$

For the purpose of satisfying Eqs. (17) and (19), taking the limiting cases $l\to 0$ and $l\to\infty$ into account, with the factor $e^{-l/a}$ introduced, equivalent straight length of wing crack can be supposed as

$$l_{\text{eq}}=\left(\frac{0.667}{\cos^2(0.5\theta)}-1\right)ae^{\frac{-l}{a}}+\frac{9}{4}l\cos^2\frac{\theta}{2}\left(1-e^{\frac{-l}{a}}\right) \tag{20}$$

In Eq.(20), taking the limiting case $l\to 0$, Eq. (20) becomes Eq. (17); taking the limiting case $l\to\infty$, Eq. (20) becomes Eq. (19). Equivalent straight length l_{eq} varies from Eq. (17) to Eq. (19) during the wing crack propagation.

Via introducing Eq. (20) into Eq. (12), we obtain the expression for mode I stress intensity factor K_{I} at the tip of wing crack subjected to hydraulic pressure and far field stresses:

$$K_{\text{I}}=3\tau_{\text{eff}}\sqrt{\frac{a+\left(\frac{0.667}{\cos^2(0.5\theta)}-1\right)ae^{\frac{-l}{a}}+\frac{9}{4}l\cos^2\frac{\theta}{2}\left(1-e^{\frac{-l}{a}}\right)}{\pi}}\cdot \sin^{-1}\left(\frac{a}{a+\left(\frac{0.667}{\cos^2(0.5\theta)}-1\right)ae^{\frac{-l}{a}}+\frac{9}{4}l\cos^2\frac{\theta}{2}\left(1-e^{\frac{-l}{a}}\right)}\right)\cdot \sin\theta\cos\frac{\theta}{2}-\frac{1}{2}[(\sigma_1+\sigma_2)+(\sigma_1-\sigma_2)\cos 2(\theta+\beta)-2p]\sqrt{\pi l} \tag{21}$$

The characteristics of wing crack model proposed are:

1) The effects of hydraulic pressure, in wing crack and in the connected part of main crack, on stress intensify factor at tip of wing crack are considered by the wing crack model proposed.

2) The whole range of variation of wing crack length from extremely short to very long can be simulated by the wing crack model proposed, and the model is definite in physical meaning.

3) In Eq. (21), if we make p=0, the model degenerates to general wing crack model.

3 Numerical analysis of wing crack propagation subjected to hydraulic pressure and far field stresses

3.1 Solution method for stress intensify factor K_{I} at wing crack tip

ANSYS is used to solve wing crack problem in fracture mechanics domain. For the analysis of a linearly elastic fracture mechanics, the tip of the crack is the singular point. Singular element is used in ANSYS. And the first row elements surrounding wing crack tip are singular elements. KSCON command assigns element division sizes around a key point. This automatically generates singular elements around the crack tip. Contact element is used to simulate the sliding of the main crack and it can satisfy the Mohr-Coulomb criterion.

The analysis of stress intensify factor K_{I} at tip of wing crack uses a fit of the nodal displacements in the vicinity of the crack. The actual displacements near a crack for linearly elastic materials are

$$u=\frac{K_{\text{I}}}{4G}\sqrt{\frac{r}{2\pi}}\left[(2k-1)\cos\frac{\theta}{2}-\cos\frac{3\theta}{2}\right]- \frac{K_{\text{II}}}{4G}\sqrt{\frac{r}{2\pi}}\left[(2k+3)\sin\frac{\theta}{2}+\sin\frac{3\theta}{2}\right]+0(r) \tag{22}$$

$$w=\frac{K_{\text{I}}}{4G}\sqrt{\frac{r}{2\pi}}\left[(2k-1)\sin\frac{\theta}{2}-\sin\frac{3\theta}{2}\right]- \frac{K_{\text{II}}}{4G}\sqrt{\frac{r}{2\pi}}\left[(2k+3)\cos\frac{\theta}{2}+\cos\frac{3\theta}{2}\right]+0(r) \tag{23}$$

where u and w are displacements in a local Cartesian coordinate system as shown in Fig. 3; r and θ are coordinates in a local cylindrical coordinate system as shown in Fig. 3; G is shear modulus; $0(r)$ presents the term of order r or higher; K_{I} is mode I stress intensity factor at the wing crack tip; K_{II} is mode II stress intensity factor at the wing crack tip. With plane strain, k=3−4ν; with plane stress, $k=\frac{3\nu}{1+\nu}$; ν is Poisson ratio.

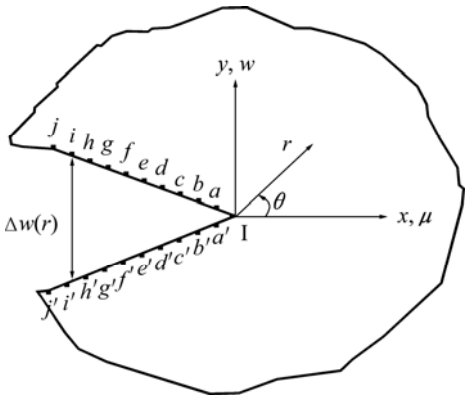

Fig. 3 Nodes used for approximate crack-tip displacements and coordinate systems

Evaluating Eq. (23) at $\theta=\pm180.0°$ and dropping the higher order terms yield

$$u=+\frac{K_{\mathrm{II}}}{2G}\sqrt{\frac{r}{2\pi}}(1+k) \tag{24}$$

$$w=+\frac{K_{\mathrm{I}}}{2G}\sqrt{\frac{r}{2\pi}}(1+k) \tag{25}$$

Model II stress intensity factor K_{II} at wing crack tip is very small, and can be disregarded, compared with model I stress intensity factor K_{I}. For full-crack model (as shown in Fig. 3), the expression for model I stress intensity factor K_{I} near the wing crack tip is

$$K_{\mathrm{I}}=\sqrt{2\pi}\frac{G}{1+k}\frac{|\Delta w|}{\sqrt{r}} \tag{26}$$

where Δw is the motion of one crack face with respect to the other, as shown in Fig. 3.

In Eq. (26), the final factor is $|\Delta w|/\sqrt{r}$, which needs to be evaluated based on the nodal displacements and locations. As shown in Fig. 3, a fit of points is available. In Eq. (26), if $r\rightarrow 0$, stress intensity factor K_{I} at the tip of wing crack is obtained:

$$K_{\mathrm{I}}=\lim_{r\to 0}\sqrt{2\pi}\frac{G}{1+k}\frac{|\Delta w|}{\sqrt{r}} \tag{27}$$

With the method of numerical simulation, stress intensify factor K_{I} at the wing crack tip can be obtained. The procedure of analysis is as follows [23]:

1) Using ANSYS, a fit of the nodal displacements near wing crack tip can be obtained.

2) Using Eq. (26), stress intensity factors $K_{\mathrm{I}}(r)$ of a fit of nodes near wing crack tip can be computed.

3) By linear fitting for stress intensity factor $K_{\mathrm{I}}(r)$ of a fit of nodes, Eq. (28) is obtained:

$$K_{\mathrm{I}}(r)=Br+A \tag{28}$$

In Eq. (28), when r=0, approximate solution of stress intensity factor at the crack tip can be obtained by numerical analysis:

$$K_{\mathrm{I}}=A \tag{29}$$

3.2 Establishment of wing crack numerical model

As shown in Fig. 4(a), the length of main crack is $\sqrt{2}$ cm, orientating an angle of 45° to the axial direction. The calculation range is set as 80 cm×160 cm and the crack is put in the middle of the model. 9 921 nodes and 3 247 elements are in the model. In the model, shear modulus G=8.3 GPa and Poisson ratio ν=0.2 are set [24].

The grids at the crack tip are refined. Uniform far field stress σ_1 is applied on top of the model while lateral stress $\sigma_2=\lambda\sigma_1$ is applied on both sides. Sliding support is set at the bottom. Hydraulic pressure αp and p are applied to inner surface of main crack and wing cracks, respectively. In order to study the evolution law of stress intensify factor at the tip of wing crack under different lateral stresses and hydraulic pressures, a certain axial compressive stress σ_1=25 MPa, combined with different lateral stresses σ_2=−2.5 MPa (λ=−0.1), 0 (λ=0), 2.5 MPa (λ=0.1) and different hydraulic pressures p= 0, 1, 3, 5 MPa are analyzed. Friction coefficient μ=0.3 of main crack surface and its connectivity rate α=0.6 are set. Suppose that wing crack propagates approximately at the direction parallel to the major applied compressive stress; accordingly, an fairly small angle between wing crack and axial stress of $\gamma=\pi/25$ is set in calculation. Wing crack numerical model and grids meshing considering the combined action of hydraulic pressure and far field stresses are shown in Fig. 4.

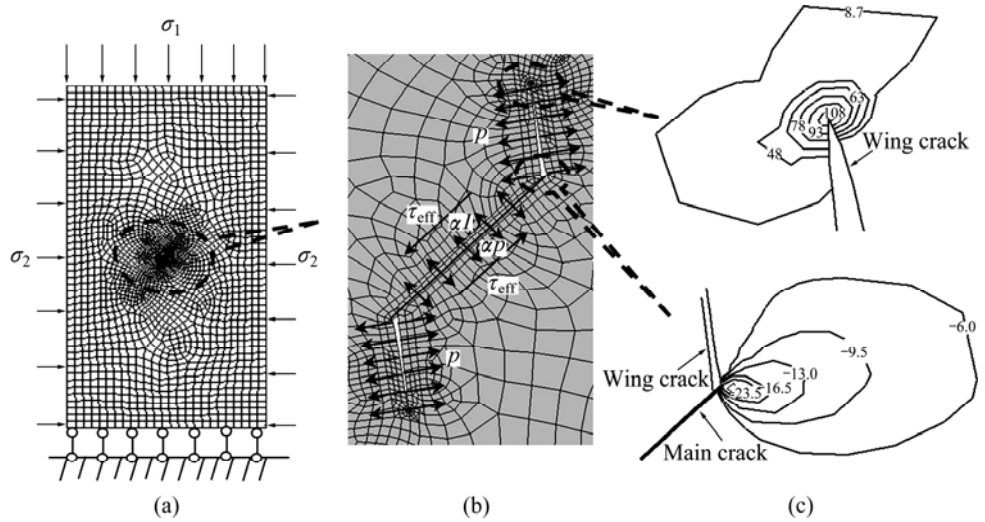

Fig. 4 Calculation model of wing crack subjected to hydraulic pressure and far field stresses: (a) Discretization of specimen for finite element analysis; (b) Sketch illustrating forces applied to main crack surface and wing crack surface; (c) Distributions of minimum principal stress σ_3 at main crack tip and wing crack tip (Unit: MPa)

3.3 Analysis of finite element method on wing crack propagation

Based on the calculation of stress intensify factor K_I at the tip of wing crack for different wing crack lengths, the procedure of wing crack propagation can be simulated subjected to hydraulic pressure and far field stresses [25].

Figure 5(a) presents the distribution of minimum principal stress around frictional crack before initiation when p=3 MPa and σ_2=0. It can be seen that tensile stress concentration at the tip of main crack is significant, and the zone of compressive concentration also locates near the tip of crack. The vector distribution of principal stress around the tip of main crack before initiation is shown in Fig. 5(b). It can be seen that the state of tensile stress concentration at the tip of main crack gives rise to the initiation of wing crack; while the state of biaxial compressive stress concentration near main crack tip causes secondary shear crack.

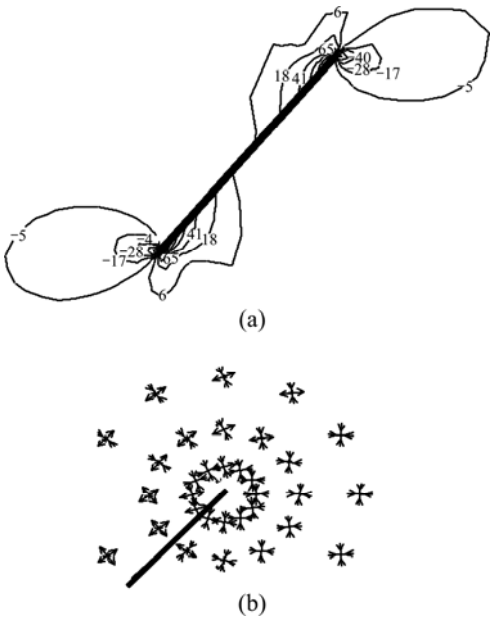

Fig. 5 Stress state around frictional main crack before initial cracking: (a) Distribution of minimum principal stress σ_3 around frictional main crack (Unit: MPa); (b) Distribution of principal stress vectors around frictional main crack

As shown in Fig. 6, a series of numerical experiments are carried out by changing the length l of wing crack when p=5 MPa and σ_2=0. By comparing these results, it can be concluded that the tensile stress concentration zone at the tip of crack does not decrease with the propagation of crack under high hydraulic pressure (p=5 MPa). On the contrary, it increases with the wing crack propagation. And the longer the wing crack is, the faster the propagation of tensile stress zone. This is mainly due to the fact that the longer the wing crack in length, the larger the area that hydraulic pressure is applied to and the stronger the splitting effect of hydraulic pressure on rock. At the same time, compressive stress concentration zone remains at the tip of main crack and its domain also increases with the propagation of wing crack.

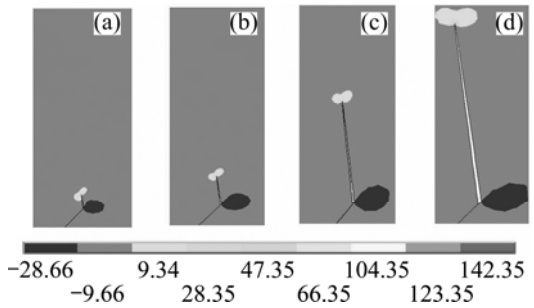

Fig. 6 Evolution of principal stress σ_3 around wing crack when p=5 MPa and σ_2=0 (Unit: MPa): (a) l=0.5 cm; (b) l=1.0 cm; (c) l=3.0 cm; (d) l=5.0 cm

For comparison, Fig. 7 shows the distributions of minimum principal stress around wing crack by changing the length l of wing crack when p=0 and σ_2=0. It can be concluded that without hydraulic pressure, tensile stress concentration zone at the tip of wing crack decreases with the propagation of the crack. Also compressive stress concentration zone at the tip of main crack has a decreasing tendency. The absolute value of minimum principal stress decreases with the propagation of the wing crack.

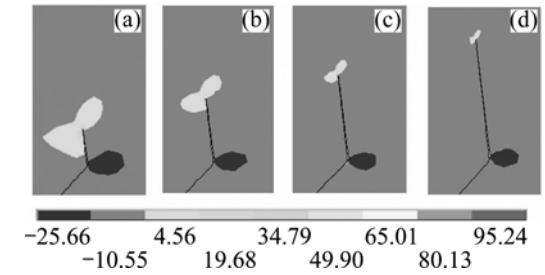

Fig. 7 Evolution of principal stress σ_3 around wing crack when p=0 and σ_2=0 (Unit: MPa): (a) l=0.5 cm; (b) l=1.0 cm; (c) l=1.5 cm; (d) l=2.0 cm

4 Evolution law of stress intensify factor K_I at tip of wing crack and comparison of theoretical model with FEM analysis

4.1 Evolution law of stress intensify factor K_I of wing crack subjected to hydraulic pressure and far field stresses

If we make L=l/a, the stress intensify factor K_I at the tip of wing crack varies with equivalent crack length L(L=l/a). The variation curves of normalized stress

intensify factor $K_I/(\sigma_1\sqrt{\pi a})$ with equivalent crack length L are obtained under different side pressure coefficients λ and hydraulic pressures p using FEM. Comparison of the curves of normalized stress intensify factor with equivalent crack length L obtained by FEM with theoretical model (Eq. (19)) is shown in Fig.8. We suppose $\theta=\pi/4+\pi/25$ in theoretical model (Eq. (21)) in order to comply with the direction in which wing crack propagates in FEM model. It can be concluded from

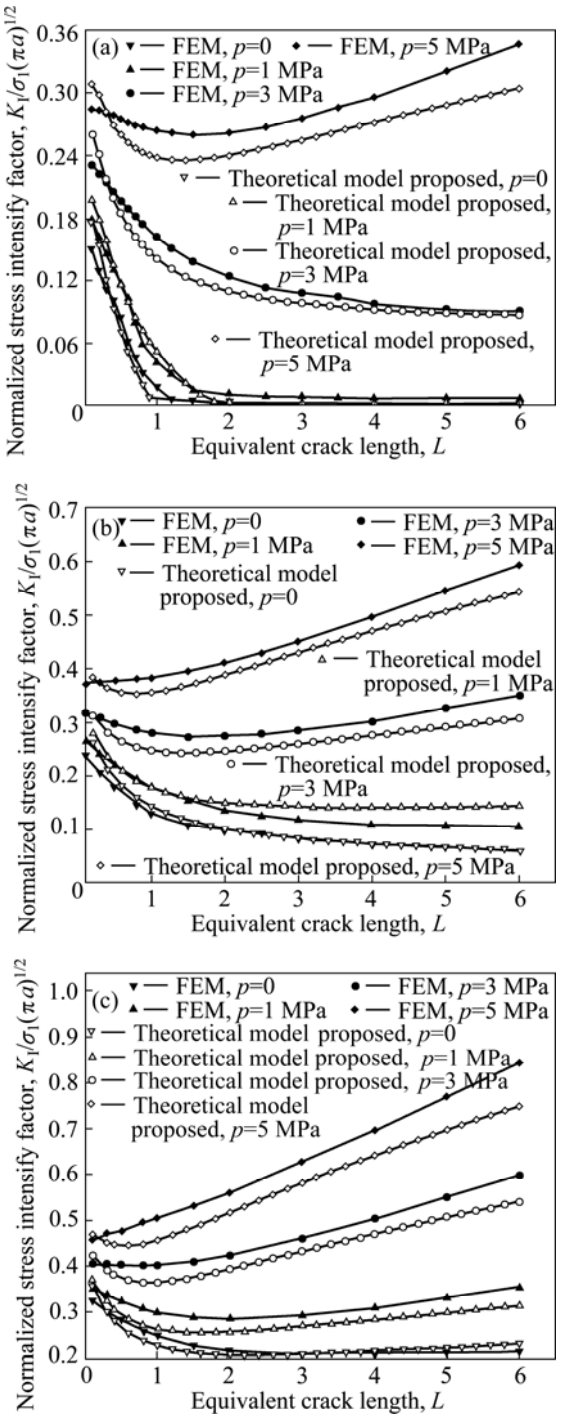

Fig. 8 Variations of normalized stress intensify factor K_I at wing crack tip with equivalent crack propagation length: (a) λ=0.1, μ=0.3; (b) λ=0, μ=0.3; (c) λ=−0.1, μ=0.3

Fig. 8 that the evolution laws of the stress intensify factor K_I at the tip of wing cracks under the combined action of hydraulic pressure and far field stresses are as follows:

1) When side pressure coefficient λ and friction coefficient μ remain constant, with the increase of hydraulic pressure p, the wing crack tends to propagate unsteadily. When λ=−0.1 and μ=0.3, if p=0, wing crack propagates steadily ($\partial K_I/\partial L<0$); if p=1, 3, and 5 MPa, respectively, wing crack propagates unsteadily, and there exists one stage of unsteady propagation in the case of $\partial K_I/\partial L>0$. With the increase of hydraulic pressure p, the stress intensify factor K_I of wing crack increases with the increment of equivalent length L. Figure 8 shows that, when hydraulic pressure p=5 MPa and side pressure coefficient λ=−0.1, 0 and 0.1, respectively, an unstable crack propagation takes place. This indicates that once frictional crack initiates, under high hydraulic pressure, wing crack will propagate fast.

2) In the case that crack distribution and hydraulic pressure are already decided but the larger side pressure coefficient λ is varied, if the stress intensify factor K_I at the tip of wing crack attenuates fast, wing crack propagates steadily. Even a relatively small lateral tensile stress (λ is negative) can induce unsteady propagation of crack (a stage of propagation with $\partial K_I/\partial L>0$).

3) The lateral tensile stress and high hydraulic pressure are the key factors that induce crack propagation unsteadily.

4.2 Comparison of theoretical model with FEM model

From Fig. 8, some errors can be found between the theoretical model of wing crack considering combined action of hydraulic pressure and far field stresses and the FEM results.

1) In general, the stress intensify factor of wing crack obtained from theoretical model is commonly lower than the result of FEM. Taking the case of p= 5 MPa and L=3.0 for example, when λ=−0.1, 0 and 0.1, the stress intensify factors K_I at the wing crack tip obtained from theoretical model are 92.6%, 95.3% and 92.4% those from FEM approach, respectively.

2) A good agreement is found between theoretical model results and FEM approach without the consideration of hydraulic pressure.

3) In condition that the length of wing crack is very little, the results of theoretical model are commonly larger than those of FEM approach.

4) The hypothesis and the equivalent wing crack length of $2l_{eq}$ proposed in theoretical mode only approximatively reveal the mechanical mechanism of the propagation of wing subjected to hydraulic pressure and far field stresses. So, some errors exist between two approaches. The theoretical model of wing crack can supply theoretical references to study of hydraulic

fracturing. The next step of our research is to apply theoretical model proposed to numerical research on coupling analysis of seepage damage fracture in fractured rock masses.

5 Conclusions

1) The new wing crack model proposed considers the combined action of hydraulic pressure and far field stresses, and takes the effect of the hydraulic pressure in wing crack and the connected part of main crack on the stress intensify factor at the tip of wing crack into consideration. The proposed model is definite in physical meaning and can simulate the whole range of variation of wing crack length from extremely short to very long.

2) With the propagation of wing crack, under high hydraulic pressure, the region of tensile stress concentration increases and the splitting effect becomes more evident.

3) The stable behavior is observed in biaxial loading when the lateral stress is compressive. In contrast, an unstable crack propagation takes place if there is high hydraulic pressure and lateral tension.

4) Though the stress intensify factor of wing crack obtained from theoretical model is commonly lower than that from FEM approach, except the case that wing crack is rather little in length, based on micromechanics, it can be deemed that good agreement is obtained between them. And the wing crack model proposed can supply theoretical references to study on hydraulic fracturing in rock masses.

References

[1] CAI M. Influence of intermediate principal stress on rock fracturing and strength near excavation boundaries—Insight from numerical modeling [J]. International Journal of Rock Mechanics & Mining Sciences, 2008, 45: 763−772.

[2] SAHOURYEH E, DYSKIN A V, GERMANOVICH L N. Crack growth under biaxial compression [J]. Eng Fract Mech, 2002, 69(18): 2187−2198.

[3] CAI M, KAISER P K. Assessment of excavation damaged zone using micromechanics model [J]. Tunnelling and Underground Space Technology, 2005, 20(4): 301−310.

[4] ASHBY M F, SAMMIS. The damage mechanics of brittle solids in compression [J]. Pageoph, 1990, 133(3): 489−518.

[5] HORII H, NEMAT-NASSER S. Compression-induced microcrack growth in brittle solids: Axial splitting and shear failure [J]. J Geophys Res, 1985, 90: 3105−3125.

[6] HORII H, NEMAT-NASSER S. Brittle failure in compression: Splitting, faulting and brittle-ductile transition [J]. Phil Trans R. Soc Lond A, 1986, 139: 337−374.

[7] ASHBY M F, HALLAM S D. The failure of brittle solids containing small cracks under compressive stress states [J]. Acta Metall, 1986, 34: 497−510.

[8] STEIF P S. Crack extension under compressive loading [J]. Engng Fract Mech, 1984, 20: 463−473.

[9] BAUD P, REUSCHLE T, CHARLEZ P. An improved wing crack model for the deformation and failure of rock in compression [J]. International Journal of Rock Mechanics and Mining Sciences and Geomechanics Abstracts, 1996, 33(5): 539−542.

[10] WANG Yuan-han, XU Yue, TAN Guo-hua. An improved calculative model for wing crack [J]. Chinese Journal of Geotechnical Engineering, 2000, 22(5): 612−615. (in Chinese)

[11] NAKASHIMA Y. Buoyancy-driven propagation of an isolated fluid-filled crack in rock: Implication for fluid transport in metamorphism [J]. Contributions to Mineralogy and Petrology, 1993, 11(4): 289−295.

[12] TANG Lian-sheng, ZHANG Peng-cheng, WANG Si-jing. Testing study on effects of chemical action of aqueous solution on crack propagation in rock [J]. Chinese Journal of Rock Mechanics and Engineering, 2002, 21(6): 822−827. (in Chinese)

[13] ZHUANG Ning. Propagation rule of crack rock mass and its mathematics model research under the hydraulic-stress coupling [D]. Shanghai: TongJi University, 2006: 111−112. (in Chinese)

[14] KATSUMI, N, HIROKAZU M, HIROAKI, N, NORIYOSHI T. Mechanical and hydraulic coupling of injection-induced slip along pre-existing fractures [J]. Geothermics, 2008, 37: 157−172.

[15] LEE M Y, HAIMSON B C. Statistical evaluation of hydraulic fracturing stress measurement parameters [J]. Int J Rock Mech Min, Sci & Geomech Abstr, 1989, 26: 447−56.

[16] LUO Xiao-rong, VASSEUR G. Natural hydraulic cracking: numerical model and sensitivity study [J]. Earth and Planetary Science Letters, 2002, 20(1): 431−446.

[17] PAPANASTASIOU P C. A coupled elastoplastic hydraulic fracturing model [J]. Int J Rock Mech & Min Sci, 1997, 34: 3−4.

[18] ZHAO Y L, CAO P, WANG W J . Viscoelasto-plastic rheological experiment under circular increment step load and unload and nonlinear creep model of soft rocks [J]. Journal of Central South University of Technology, 2009, 16(3): 484−491.

[19] LAUTERBACH B, GROSS D. Crack growth in brittle solids under compression [J]. Mechanics of Materials, 1998, 29: 81−92.

[20] LEE S, RABICHANDRAN G. Crack initiation in brittle solids under multiaxial compression [J]. Engineering Fracture Mechanics, 2003, 70: 1645–1658.

[21] DYSKIM A V, SAHOURYEH E, JEWELL R J, JOER J H, USTINOV K B. Influence of shape and locations of initial 3-D cracks on their growth in uniaxial compression [J]. Engineering Fracture Mechanics, 2003, 70: 2115–2136.

[22] SAHOURYEH E, DYSKIM A V, GERMANOVICH L N. Crack growth under biaxial compression [J]. Engineering Fracture Mechanics, 2002, 69: 2187–2198.

[23] YU Xiao-zhong. Fracture mechanics of rock and concrete [M]. Changsha: Central South University of Technology Press, 1991: 20−21. (in Chinese)

[24] AYATOLLAHI M R, ALIHA M R M. Wide range data for crack tip parameters in two disc-type specimens under mixed model loading [J]. Computational Materials Science, 2007, 38(4): 660−670.

[25] ZHAO Yan-lin, CAO Ping, WEN You-dao. Damage fracture failure mechanism of compressive-shear rock cracks under seepage pressure [J]. Journal of Central South University: Science and Technology, 2008, 39(4): 838−844. (in Chinese)

(Edited by YANG Bing)